Supplementary Notes

Wing-tail coordination balances efficient cruising and maneuvering flight in an avian-inspired flapping robot

Supplementary Note 1

Predictive aerodynamic model coefficients and parameters

The predictive aerodynamic model used in the main text is implemented using empirical quadratic response surfaces for the wing-body assembly and tail, together with an additional tail axial-force correction term. The response-surface forms and all variables, coupling parameters and polynomial coefficients used in the calculations are provided below.

$$\text{Wing-body model: } Q_{wb} = c0 + c1\,V + c2\,a_{wb} + c3\,f + c4\,V^2 + c5\,a_{wb}^2 + c6\,f^2 + c7\,V\,a_{wb} + c8\,V\,f + c9\,a_{wb}\,f \quad (1)$$

$$\text{Tail model: } Q_t = c0 + c1\,S_t + c2\,V_t + c3\,a_t + c4\,S_t^2 + c5\,V_t^2 + c6\,a_t^2 + c7\,S_t\,V_t + c8\,S_t\,a_t + c9\,V_t\,a_t \quad (2)$$

$$\text{Tail thrust correction: } T_t = c0 + c1\,V + c2\,f + c3\,a_{wb} + c4\,i_t + c5\,S_t + c6\,a_{wb}^2 + c7\,V\,a_{wb} + c8\,V\,i_t + c9\,V\,S_t + c10\,f\,a_{wb} + c11\,a_{wb}\,i_t + c12\,a_{wb}\,S_t + c13\,f\,i_t + c14\,i_t\,S_t \quad (3)$$

Supplementary Table 1 | Definition of variables and model outputs.

Symbol	Definition	Unit used in model	Notes
V	Freestream velocity	m s^-1	Input variable
f	Flapping frequency	Hz	Input variable
α	Full-vehicle angle of attack	deg	Defined with respect to freestream
a_{wb}	Effective angle of attack of wing	deg	$a_{wb} = \alpha + i_{w,p}$
$i_{w,p}$	Mean flapping-wing incidence angle	deg	Used for pitch/lift modulation
$i_{w,r}$	Differential flapping-wing incidence angle	deg	Used for roll control; not included in the cycle-averaged longitudinal model
i_t	Tail installation angle	deg	Negative value denotes negative-installation-angle tail
S_t	Tail area	mm^2	Tail area used directly in the supplied MATLAB coefficients
V_t	Local inflow velocity at the tail	m s^-1	$V_t = \gamma V$
a_t	Effective angle of attack of tail	deg	$a_t = \alpha + i_t + e$
e	Induced downwash angle at the tail	deg	$e = e0 + (de/d\alpha)\,a_{wb}$
η	Dynamic pressure ratio at the tail	–	$\eta = V_t^2/V^2$
γ	Velocity ratio at the tail	–	$\gamma = \mathrm{sqrt}(\eta)$
L_{wb}, T_{wb}, M_{wb}	Wing-body lift, thrust and pitching moment	g, g, g mm	Cycle-averaged values
L_t, D_t, M_t	Tail lift, drag and pitching moment	g, g, g mm	Calculated by the tail model
T_t	Tail axial-force correction term	g	Additional correction term for the complete-robot thrust model

Supplementary Table 2 | Coupling and correction parameters used in the integrated aerodynamic model.

Parameter	Definition	Value	Unit	How used
$e0$	Constant term of induced downwash angle	1.670914	deg	$e = e0 + (de/d\alpha)\,a_{wb}$

Parameter	Definition	Value	Unit	How used
de/dα	Downwash gradient with respect to a_wb	-0.402524	deg deg^-1	e = e0 + (de/dα) a_wb
η	Dynamic pressure ratio at tail	1.139832	–	η = V_t^2/V^2
γ	Velocity ratio at tail	1.067629149	–	V_t = γV

Supplementary Table 3 | Polynomial coefficients of the wing-body aerodynamic model.

Term	Basis function	L_wb coefficient	T_wb coefficient	M_wb coefficient
c0	1	-39.48229	9.919843	3458.266
c1	V	8.402958	-6.889754	-874.6396
c2	a_wb	1.536976	1.564549	15.46113
c3	f	1.576298	4.436373	-77.2264
c4	V^2	-0.05138887	0.4576375	23.64245
c5	a_wb^2	-0.1015594	-0.04088336	1.074374
c6	f^2	0.1635322	0.002467255	-5.595821
c7	V*a_wb	0.5803927	-0.2124357	-30.08383
c8	V*f	-0.45504	-0.2573412	19.87128
c9	a_wb*f	0.1716213	-0.1027089	-7.003613

Note: The basis functions are ordered as [1, V, a_wb, f, V^2, a_wb^2, f^2, V*a_wb, V*f, a_wb*f]. Outputs are g for L_wb and T_wb, and g mm for M_wb.

Supplementary Table 4 | Polynomial coefficients of the tail aerodynamic model.

Term	Basis function	L_t coefficient	D_t coefficient	M_t coefficient
c0	1	2.665533e-13	0.2623304	-2.679879e-11
c1	S_t	-3.978323e-17	-0.00012115	6.713856e-15
c2	V_t	-5.382916e-15	-0.3027891	-3.803459e-12
c3	a_t	-7.015105	-4.967286e-17	1454.099
c4	S_t^2	1.342770e-21	2.337728e-09	-2.616236e-19
c5	V_t^2	-2.098771e-16	0.01360224	2.267338e-13
c6	a_t^2	-1.050223e-17	0.02395242	1.097795e-15
c7	S_t*V_t	6.408263e-19	3.248159e-05	7.810510e-18
c8	S_t*a_t	0.000355839	3.818053e-21	-0.07578285
c9	V_t*a_t	0.5988123	-1.532581e-19	-128.9571

Note: The basis functions are ordered as [1, S_t, V_t, a_t, S_t^2, V_t^2, a_t^2, S_t*V_t, S_t*a_t, V_t*a_t]. Outputs are g for L_t and D_t, and g mm for M_t.

Supplementary Table 5 | Polynomial coefficients of the tail thrust correction term.

Term	Basis function	T_t,corr coefficient
c0	1	-19.415944
c1	V	5.842321
c2	f	-4.382996
c3	a_wb	-4.489071
c4	i_t	-2.041676
c5	S_t	-0.000853
c6	a_wb^2	0.135865
c7	V*a_wb	0.588539
c8	V*i_t	0.372044
c9	V*S_t	0.000194

Term	Basis function	T_t,corr coefficient
c10	f*a_wb	0.06924
c11	a_wb*i_t	0.089084
c12	a_wb*S_t	3.400000e-05
c13	f*i_t	-0.120164
c14	i_t*S_t	4.700000e-05

Note: The basis functions are ordered as [1, V, f, a_wb, i_t, S_t, a_wb^2, V*a_wb, V*i_t, V*S_t, f*a_wb, a_wb*i_t, a_wb*S_t, f*i_t, i_t*S_t]. The correction is used as an additional axial-force/thrust term in the complete-robot model.

Supplementary Note 2

Sensitivity of aerodynamic-center migration and Pareto design conclusions

Quantitative discrepancy in aerodynamic-center migration

Aerodynamic-center position is determined by the angle-of-attack derivatives of complete-robot lift and pitching moment. The predictive model captures the direction and relative ordering of aerodynamic-center migration among the three wing-tail control strategies, but overpredicts the migration magnitude relative to the full-vehicle wind-tunnel measurements in Fig. 4d. The discrepancy is more pronounced in the pitching-moment slope and is associated with the simplified treatment of the incremental aerodynamic response induced by tail morphing.

$$x\_AC = -(\partial M/\partial \alpha)/(\partial L/\partial \alpha) = -M\_\alpha/L\_\alpha \quad (4)$$

Sensitivity perturbation and results

To test whether this quantitative discrepancy affects the Pareto-design conclusions, the model was not refitted. Using the median tail area S_ref as the reference state, a dimensionless factor k_t was applied only to the incremental aerodynamic sensitivity associated with tail-area variation:

$$Q\_t\text{^}sens = Q\_t\text{^}nominal + (k\_t - 1)\ C\_S\alpha\ (S\_t - S\_ref)\ \alpha\_t \quad (5)$$

Here, k_t = 1 recovers the nominal model, whereas k_t = 0.75 and 0.5 represent moderate and conservative lower-bound perturbations. The reference aerodynamic forces, moments and trim state are unchanged. At k_t = 0.5, the tail-morphing-only aerodynamic-center migration approaches the experimental result; this value is used only for robustness testing and not as a model recalibration.

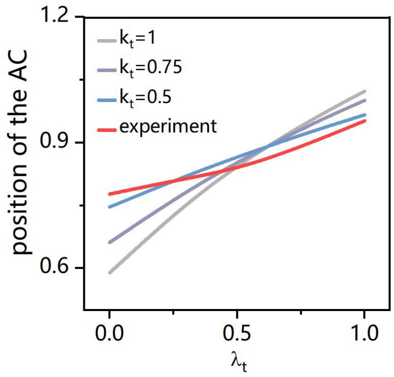

Supplementary Fig. 1 | Effect of the sensitivity scaling factor on aerodynamic-center migration for the tail-morphing-only strategy. The red line denotes the full-vehicle wind-tunnel result; k_t = 1, 0.75 and 0.5 denote the nominal, moderate and lower-bound perturbations, respectively.

The perturbations produce only limited shifts in the Pareto trajectories. The overall cruise-maneuver trade-off, the relative performance ordering of the configurations, and the wing-tail coordination logic remain essentially unchanged. The largest sensitivity occurs in the zero-lift pitching moment and the corresponding longitudinal static-stability boundary. Thus, -10° is not interpreted as a unique mathematical optimum, but it remains within the statically stable region while retaining high maneuvering capability across the examined perturbations.

Pareto-design sensitivity

a

k_t = 1

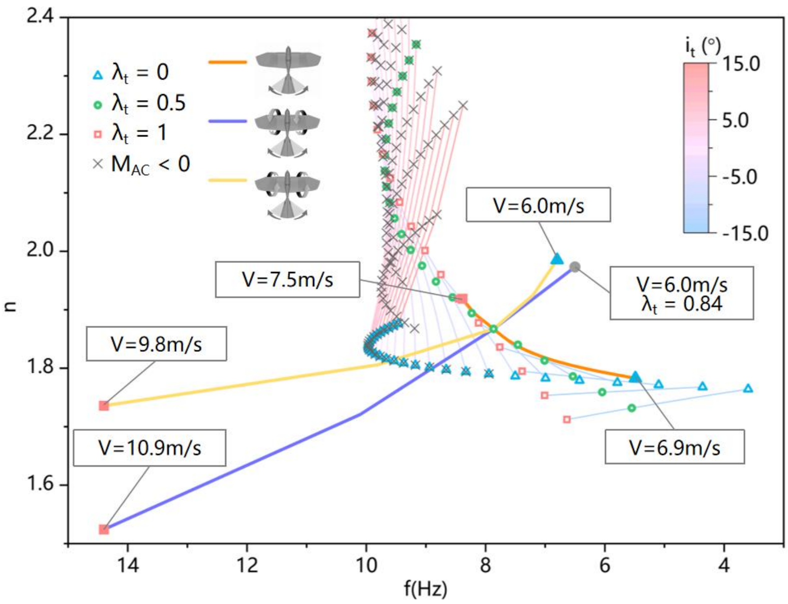

b

k_t = 0.75

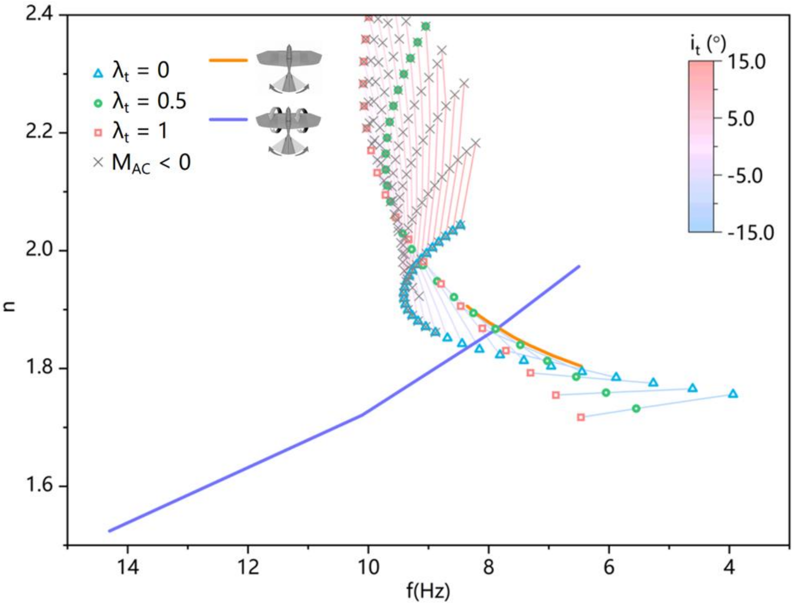

c

k_t = 0.5

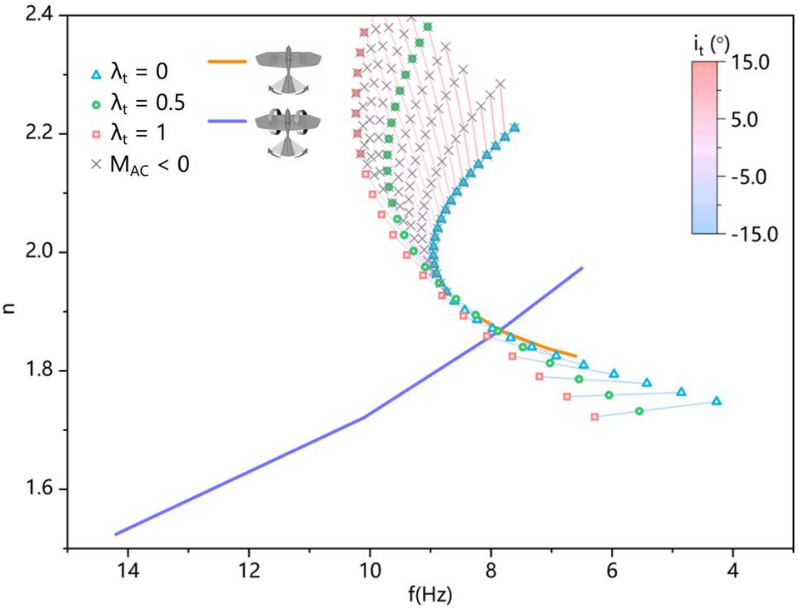

Supplementary Fig. 2 | Pareto design space under different sensitivity scaling factors. a, $k_t = 1$ (nominal model). b, $k_t = 0.75$. c, $k_t = 0.5$. Reducing the incremental aerodynamic sensitivity causes only limited shifts of the Pareto trajectories, while the overall cruise-maneuver trade-off and the relative performance relationship of the wing-tail coordination strategies are preserved.

Conclusion

The quantitative discrepancy in aerodynamic-center migration mainly affects the longitudinal static-stability boundary and the location of the exact optimum tail installation angle. It does not alter the fundamental cruise-maneuver trade-off, the performance migration produced by tail morphing, or the performance-space extension obtained by coordinating tail extension with flapping-wing supination. The -10° configuration is therefore treated as a practical design point with sufficient longitudinal static-stability margin and high maneuvering capability, rather than as a unique mathematical optimum.